

Article

Efficient Joint Estimation of Carrier Frequency and Sampling Frequency Offsets for MIMO-OFDM ATSC Systems

Yong-An Jung and Young-Hwan You *

Department of Computer Engineering, Sejong University, Gwangjin-gu, Gunja-dong 98, Seoul 05006, Korea; plar1054@naver.com

* Correspondence: yhyou@sejong.ac.kr; Tel.: +82-2-3408-3737

Received: 8 October 2018; Accepted: 25 October 2018; Published: 29 October 2018



Abstract: Multiple-input multiple-output orthogonal frequency division multiplexing (MIMO-OFDM) is appealing for the provision of high spectral efficiency in digital terrestrial broadcast systems. To fully obtain its advantageous features, it is very important to remove the frequency mismatch between the transmitter and the receiver. In this paper, we present the performance analysis of joint estimation of carrier and sampling frequency offsets in the MIMO-OFDM-based advanced television systems committee (ATSC) 3.0 system. In the MIMO-OFDM ATSC system, the continual pilot (CP) is primarily utilized to perform frequency synchronization. To efficiently suppress an unwanted bias introduced by the presence of random-likely located CPs, an optimal pilot subset is selected to form the basis of least squares frequency-offset estimation. A closed-form mean squared error is derived in the context of MIMO-OFDM, considering the multipath fading channel. We show via computer simulations and numerical analysis that the proposed estimation method achieves higher estimation accuracy than the existing estimation method.

Keywords: Multiple-input multiple-output orthogonal frequency division multiplexing (MIMO-OFDM); advanced television systems committee (ATSC) 3.0; frequency offset; pilot subset

1. Introduction

Orthogonal frequency division multiplexing (OFDM) has been successfully applied in many high data rate communication systems because of its attractive spectrum usage efficiency. Due to its benefits of wide available bandwidth, OFDM has been considered for optical communication systems. Optical OFDM can be used for short and long distance applications such as optical access networks, multimode fiber transmissions, free space optical systems, and indoor visible light communications [1–5]. In the broadcasting domain, the use of OFDM modulation facilitates the deployment of single frequency networks (SFN) in numerous broadcast systems such as digital radio mondiale (DRM), digital video broadcasting-terrestrial-second generation (DVB-T2), DVB next-generation handheld (DVB-NGH) systems, integrated services digital broadcasting-terrestrial (ISDB-T) systems, and the advanced television systems committee (ATSC) 3.0 [6–10]. DVB-T2 was designed primarily to provide interactive content that requires high bandwidth, such as HDTV and 3D TV [11]. To support these requirements, the DVB-T2 standard has incorporated a widely used multiple-input single-output (MISO) antenna scheme [7]. The DVB-NGH system is the first broadcast standard to integrate a multiple-input multiple-output (MIMO) scheme in order to increase bandwidth efficiency without any need for extra wireless bandwidth [12]. Recently, ATSC 3.0 and ISDB-T have adopted MIMO to achieve higher throughput and increase coverage [13,14]. Many studies have been carried out to improve MIMO configurations and transceivers in digital terrestrial broadcast systems [14–16].

Despite many advantageous features, the OFDM-based ATSC 3.0 system has a few key issues that have to be addressed. One of the biggest weaknesses of OFDM is its vulnerability to synchronization mismatches, including symbol timing offset (STO), carrier frequency offset (CFO), and sampling frequency offset (SFO) in a frequency-selective fading environment [17]. If these effects are not properly compensated, OFDM systems can suffer from severe inter-symbol interference (ISI) or inter-channel interference (ICI), which downgrades the performance of OFDM and MIMO-OFDM systems. To eliminate ICI and ISI effects, the receiver must first estimate the correct STO [18,19]. Second, it is essential that the frequency offset on the OFDM block is estimated and corrected to remove ICI. In particular, the performance of OFDM receivers is greatly affected by SFO as the fast Fourier transform (FFT) size becomes larger [20], which usually occurs in a typical broadcast system. Therefore, the challenges in the MIMO-OFDM-based ATSC 3.0 system are its susceptibility to the frequency synchronization between the transmitter and the receiver. In order to help acquire synchronization, the ATSC 3.0 system provides several types of pilot symbols such as scattered pilots (SPs), edge pilots (EPs), continual pilots (CPs), and subframe boundary pilots (SBPs) [10]. The SPs, EPs, and SBPs are mainly dedicated to estimate the channel, whereas CPs are present to assist time and frequency estimation [21]. To maximize the advantages of MIMO-OFDM, it is therefore of crucial importance to accurately estimate the CFO and SFO [22,23]. In the literature, a number of pilot-assisted approaches, from maximum likelihood estimation (MLE) to linear least-squares estimation (LSE) strategies [22–35], have been presented to obtain accurate CFO and SFO estimates. The MLE is well known to be capable of achieving high accuracy in joint estimation of CFO and SFO, but its high complexity limits its practical use [22–25]. To solve the complexity issue, a considerable amount of research has been devoted to the low complexity variants of joint MLE [26–35]. In [26–32], the ad-hoc-based CFO and SFO estimation strategy was developed calculating the phase difference from two consecutive pilot symbols with symmetric and uniform distribution across DC. In [33–35], a decoupled estimation of CFO and SFO was proposed, which is still computation-intensive for real-time processing. Hence, more efficient frequency estimation and its complete performance analysis in a multipath fading channel is a key challenge in realizing high-performance MIMO-OFDM receivers.

In this paper, the performance analysis of joint CFO and SFO estimator for the MIMO-OFDM ATSC broadcast system is presented in a the multipath fading channel. The CPs are used for the purpose of synchronization, and an optimal CP subset is searched to form the basis of robust estimation. The choice of the optimal pilot subset plays an important role on removing a bias produced by using random-likely distributed CPs. To assess the usefulness of the proposed LSE method, the mean squared error (MSE) is theoretically derived for the MIMO-OFDM ATSC system in a frequency-selective fading channel. It is demonstrated from numerical analysis that the joint estimation scheme using optimal pilot subset offers a robust estimation performance with a low computational burden, in comparison to the existing method.

This paper is structured as follows. Section 2 describes the signal model in the MIMO-OFDM ATSC system. In Section 3, the existing LSE method is applied to the MIMO-OFDM ATSC system. In Section 4, an improved LSE method is presented and the MSE performance is numerically analyzed in the MIMO-OFDM ATSC system. The simulation results and discussions showing the advantages of the proposed LSE method are presented in Section 5. Section 6 concludes this paper.

The notations used in this paper are listed as follows. $|\cdot|$, $(\cdot)^*$, $E\{\cdot\}$, and $(\cdot)^Q$ denote the operations taking the absolute value, complex conjugation, expectation, and real part of enclosed quantity, respectively. \angle and \otimes indicate the radian angle and convolution operators. The imaginary unit is $j = \sqrt{-1}$.

2. System Description

Consider a MIMO-OFDM system having N_u non-zero subcarriers, N_R receive antennas, and N_T transmit antennas. The frequency-domain signal is transformed by N -point inverse FFT (IFFT) to generate the time-domain signal and a guard interval (GI) with N_g samples is appended to the front of

the OFDM symbol to combat ISI. The n -th sample transmitted from transmit antenna m during the l -th period can then be written by

$$x_l^m(n) = \frac{1}{\sqrt{N_T}} \sum_{k=-N/2}^{N/2-1} X_l^m(k) e^{j2\pi kn/N}, \quad n = -N_g, -N_g + 1, \dots, N - 1 \quad (1)$$

where $X_l^m(k)$ is a complex signal from transmit antenna m at subcarrier k with symbol energy $E_X = |X_l^m(k)|^2$ and the normalization factor $1/\sqrt{N_T}$ is used to keep the transmission power constant. As a consequence, one OFDM symbol of effective duration $T_s = N_s T$ is generated, where T is the sampling time and $N_s = N + N_g$. In the frequency domain, $N - N_u$ subcarriers are zero-padded. The continuous-time baseband signal transmitted at antenna m is expressed as

$$\begin{aligned} x^m(t) &= \sum_{l=0}^{\infty} x_l^m(t) \\ &= \sum_{l=0}^{\infty} \sum_{k=-N/2}^{N/2-1} X_l^m(k) e^{j2\pi(k/T_s)(t-T_g-lT_s)} s(t-lT_s) \end{aligned} \quad (2)$$

where T_g is the GI duration and $s(t)$ is the shaping pulse given as

$$s(t) = \begin{cases} 1, & 0 \leq t \leq T_s \\ 0, & \text{otherwise} \end{cases} \quad (3)$$

Figure 1 depicts the block diagram of the MIMO-OFDM receiver including the synchronization block. Since the frequency of the local oscillator f_c' is not exactly matched to the received carrier frequency f_c , the time-domain signal in receiver antenna r can be given by

$$y^r(t) = e^{j2\pi(f_c' - f_c)t} \sum_{m=1}^{N_T} x^m(t) \otimes h^{m,r}(t) + z^r(t), \quad r = 1, 2, \dots, N_R \quad (4)$$

where $f_c' - f_c$ means the CFO in Hz, $h^{m,r}(t)$ is the channel impulse response (CIR) from transmit antenna m to receive antenna r , and $z^r(t)$ is a zero-mean additive white Gaussian noise (AWGN) process at receive antenna r . In Equation (4), $h^{m,r}(t)$ takes the form

$$h^{m,r}(t) = \sum_{p=0}^{P-1} \alpha_p^{m,r} \delta(t - \tau_p^{m,r}) \quad (5)$$

where P is the number of multipaths, and $\alpha_p^{m,r}$ and $\tau_p^{m,r}$ denote the attenuation and delay of the p -th multipath from transmit antenna m to receive antenna r , respectively. Since the multiple antennas are usually co-located, only one oscillator is referenced in either the transmit side or receiver side. Moreover, the differences in Doppler shift between all transmit–receive antenna pairs are small in typical broadcasting systems. With those implications in mind, we consider scenarios where all transmit–receive antenna couples experience a single common CFO and SFO as discussed in [36–38].

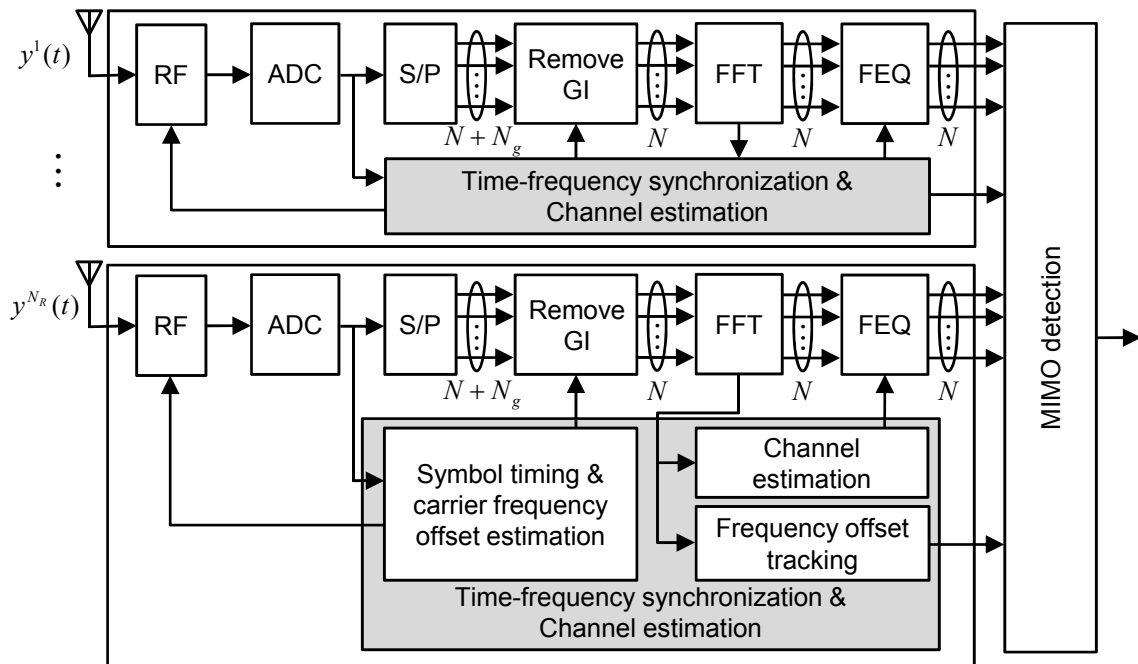


Figure 1. System model of the multiple-input multiple-output orthogonal frequency division multiplexing-based advanced television systems committee (ATSC) receiver.

The received signal $y^r(t)$ is sampled at time instants $t = nT'$, which leads to a SFO $\xi = (T' - T)/T$. At the receiver, the sampled signal at time instants $t = nT'$ becomes [34]

$$y^r(nT') = e^{2\pi\epsilon nT'/NT} \sum_{m=1}^{N_T} \sum_p h_p^{m,r}(nT') x^m(nT' - \tau_p^{m,r}) + z^r(nT'), \quad r = 1, 2, \dots, N_R \quad (6)$$

where ϵ is the normalized CFO by the subcarrier spacing $1/NT$, and $h_p^{m,r}(nT')$ and $z^r(nT')$ are the samples of multiplicative channel and additive noise, respectively. As shown in Figure 1, the estimation of initial STO and CFO is performed during pre-FFT phase, which is usually based on the inherent redundant information in OFDM symbols. After FFT, residual CFO and SFO are estimated and tracked using either CP or SP. After the time and frequency synchronization process, the receiver performs channel estimation and MIMO detection in a sequential or iterative manner [39]. Since this paper focuses on the post-FFT synchronization processing, we consider the situation where coarse CFO estimation has been done before FFT is performed. In addition, we assume the perfect knowledge of the STO at the receiver. After discarding the GI and performing N -point FFT for the l -th OFDM symbol, the received OFDM signal in receiver antenna r at subcarrier k appears as

$$Y_l^r(k) = \frac{1}{N} \sum_{n=0}^{N-1} y^r((n + N_g + lN_s)T') e^{-j2\pi kn/N}, \quad r = 1, 2, \dots, N_R, \quad (7)$$

which is further derived as [33,34]

$$Y_l^r(k) = \frac{1}{\sqrt{N_T}} \sum_{m=1}^{N_T} \beta(k) H_l^{m,r}(k) X_l^m(k) e^{j2\pi\varphi(k)(lN_s + N_g)/N} + C_l^r(k) + Z_l^r(k), \quad r = 1, 2, \dots, N_R \quad (8)$$

where $\varphi(k) = \epsilon + k\xi$, $\beta(k) = \sin(\pi(\varphi(k))/N) \sin(\pi\varphi(k)/N)$, $H_l^{m,r}(k)$ is the equivalent channel transfer function (CTF) from transmit antenna m to receive antenna r with variance σ_H^2 , $C_l^r(k)$ is a zero-mean complex ICI with variance σ_C^2 at receive antenna r , and $Z_l^r(k)$ is a zero-mean complex AWGN with variance σ_Z^2 at receive antenna r . For typical values of ϵ and ξ , $\beta(k) \approx 1$ and $\sigma_C^2 \approx E_X \sigma_H^2 \epsilon^2 \pi^2 / 3$ [17]. Since the same common CPs are transmitted from the transmit antennas in the MIMO-OFDM ATSC

system [10], an equivalent CTF at the receive antenna r can be treated as a sum of CTFs from N_T transmit antennas

$$H_l^r(k) = \frac{1}{\sqrt{N_T}} \sum_{m=1}^{N_T} H_l^{m,r}(k), \quad (9)$$

which is modeled as a complex zero-mean Gaussian process with variance σ_H^2 .

3. The Conventional LSE Scheme

Since many pilot symbols are dedicated to the purpose of time and frequency synchronization in the ATSC 3.0 system, we focus on the pilot-based LSE scheme [28–31] as a reference to the proposed method. In this paper, we consider the common CPs as pilot symbols, which are continuously inserted at a fixed subcarrier position. The channel is assumed to remain stationary during two symbol periods so that $H_l^{m,r}(k) = H_{l+1}^{m,r}(k)$. We omit the superscript m in $H_l^m(k)$ assuming that the pilot symbols are the same among the transmit antennas. Based upon two consecutive CPs, the pilot-compensated signals in the MIMO configuration is represented by

$$\begin{aligned} \tilde{Y}_l(k) &= \sum_{r=1}^{N_R} Y_l^{r*}(k) X_l(k) Y_{l+1}^r(k) X_{l+1}^*(k) \\ &= \sum_{r=1}^{N_R} |H_l^r(k)|^2 E_X^2 e^{j2\pi\varphi(k)\rho} + \sum_{r=1}^{N_R} \tilde{C}_l^r(k) + \sum_{r=1}^{N_R} \tilde{Z}_l^r(k), \quad k \in \mathcal{S}_f \end{aligned} \quad (10)$$

where $\rho = N_s/N$, \mathcal{S}_f is the set of pilot subcarrier indices, $\tilde{C}_l^r(k)$ is the ICI component written as

$$\begin{aligned} \tilde{C}_l^r(k) &= E_X H_l^{r*}(k) X_{l+1}^*(k) C_{l+1}^r(k) e^{-j2\pi\varphi(k)(lN_s+N_g)/N} \\ &\quad + E_X H_{l+1}^r(k) X_l(k) C_l^{r*}(k) e^{j2\pi\varphi(k)((l+1)N_s+N_g)/N} + C_{l+1}^r(k) Z_l^{r*}(k) X_l(k) X_{l+1}^*(k), \\ &\quad + C_l^{r*}(k) Z_{l+1}^r(k) X_l(k) X_{l+1}^*(k) + C_{l+1}^r(k) C_l^{r*}(k) X_l(k) X_{l+1}^*(k) \end{aligned} \quad (11)$$

and $\tilde{Z}_l^r(k)$ is the AWGN component written as

$$\begin{aligned} \tilde{Z}_l^r(k) &= E_X H_l^{r*}(k) X_{l+1}^*(k) Z_{l+1}^r(k) e^{-j2\pi\varphi(k)(lN_s+N_g)/N} \\ &\quad + E_X H_{l+1}^r(k) X_l(k) Z_l^{r*}(k) e^{j2\pi\varphi(k)((l+1)N_s+N_g)/N} + Z_l^{r*}(k) Z_{l+1}^r(k) X_l(k) X_{l+1}^*(k). \end{aligned} \quad (12)$$

For notation simplicity, the argument of $\tilde{Y}_l(k)$ takes the form

$$\angle \tilde{Y}_l(k) = 2\pi\rho\varphi(k) + I_l(k) \quad (13)$$

where $I_l(k)$ means an appropriate noise term after taking an argument. When the common CPs are entirely used for synchronization, the CFO and SFO are obtained by applying the LS regression to $\varphi(k) = \varepsilon + k\zeta$ as

$$\begin{aligned} \hat{\varepsilon} &= \frac{1}{2\pi\rho N_f} \sum_{k \in \mathcal{S}^+ \cup \mathcal{S}^-} \angle \tilde{Y}_l(k) \\ &= \varepsilon + \frac{1}{2\pi\rho N_f} \sum_{k \in \mathcal{S}^+ \cup \mathcal{S}^-} I_l(k) + \frac{\zeta A_f}{N_f} \end{aligned} \quad (14)$$

and

$$\begin{aligned}\hat{\xi} &= \frac{1}{2\pi\rho M_f} \sum_{k \in \mathcal{S}^+ \cup \mathcal{S}^-} k \angle \tilde{Y}_l(k) \\ &= \xi + \frac{1}{2\pi\rho M_f} \sum_{k \in \mathcal{S}^+ \cup \mathcal{S}^-} k I_l(k) + \frac{\varepsilon A_f}{M_f}\end{aligned}\quad (15)$$

where \mathcal{S}^+ denotes the set of positive CP subcarriers containing N^+ members, \mathcal{S}^- denotes the set of negative CP subcarriers containing N^- members, $N_f = N^+ + N^-$ stands for the total number of pilot subcarriers present in $\mathcal{S}_f = \mathcal{S}^+ \cup \mathcal{S}^-$, $A_f = \sum_{k \in \mathcal{S}^+ \cup \mathcal{S}^-} k$, and $M_f = \sum_{k \in \mathcal{S}^+ \cup \mathcal{S}^-} k^2$. Note that the second term of the right-hand side (RHS) of Equations (14) and (15) is the intrinsic interference caused by AWGN and ICI, whereas the third term is the extra bias introduced by the existence of non-symmetrically located CPs. Among them, the interferences due to ICI and CPs do not vanish even as signal-to-noise ratio (SNR) grows.

Since CPs are randomly distributed in the ATSC 3.0 system, it is not guaranteed that $A_f = 0$. In such a case, an unwanted bias can be occurred by non-symmetrically distributed CPs, which leads to an irreducible MSE floor. To account for this issue, an effective LSE scheme is suggested based on a pilot subset selection in the following section.

4. The Proposed LSE Scheme

This section presents an effective joint CFO and SFO estimation scheme in the MIMO-OFDM ATSC system and its performance analysis is presented in the multipath fading channel. The improved CFO and SFO estimation scheme is achieved by properly choosing a pilot subset so that a bias incurred by using randomly distributed CPs can be eliminated.

4.1. Pilot Selection

Let \mathcal{S}_b^+ and \mathcal{S}_b^- be the searched optimal subsets for positive and negative subcarrier frequencies around DC, respectively. The argument over the pilot-compensated signal $\tilde{Y}_l(k)$ is then decomposed as

$$\begin{aligned}\Lambda_1 &= \sum_{k \in \mathcal{S}_b^+} \angle \tilde{Y}_l(k) + \sum_{k \in \mathcal{S}_d^-} \angle \tilde{Y}_l(k) \\ &= 2\pi\rho\varepsilon N_p + \sum_{k \in \mathcal{S}_b^+ \cup \mathcal{S}_d^-} I_l(k) + 2\pi\rho\xi A_p\end{aligned}\quad (16)$$

with

$$A_p = \sum_{k \in \mathcal{S}_b^+} k + \sum_{k \in \mathcal{S}_d^-} k \quad (17)$$

where $\mathcal{S}_b^+ \in \mathcal{S}^+$ contains the N_b^+ elements, $\mathcal{S}_d^- \in \mathcal{S}^-$ contains the N_d^- elements, and $N_p = N_b^+ + N_d^-$ is the number of CPs utilized in the proposed estimation scheme. Similarly, we have

$$\begin{aligned}\Lambda_2 &= \sum_{k \in \mathcal{S}_b^+} k \angle \tilde{Y}_l(k) + \sum_{k \in \mathcal{S}_d^-} k \angle \tilde{Y}_l(k) \\ &= 2\pi\rho\xi M_p + \sum_{k \in \mathcal{S}_b^+ \cup \mathcal{S}_d^-} k I_l(k) + 2\pi\rho\varepsilon A_p\end{aligned}\quad (18)$$

where

$$M_p = \sum_{k \in \mathcal{S}_b^+} k^2 + \sum_{k \in \mathcal{S}_d^-} k^2. \quad (19)$$

In order to independently estimate the CFO and SFO using Equations (16) and (18), A_p should be zero because of non-zero valued SFO and CFO in the third term of the RHS of Equations (16) and (18), respectively. In this paper, the goal of the pilot subset selection scheme is to make A_p zero as well as maximize N_p and M_p at the same time. For this purpose, two subsets \mathcal{S}_b^+ and \mathcal{S}_d^- are selected to meet the following criteria:

$$(\hat{b}, \hat{d}) = \underset{1 \leq b \leq C_+, 1 \leq d \leq C_-}{\text{arg zero}} \left\{ \sum_{k \in \mathcal{S}_b^+} k + \sum_{k \in \mathcal{S}_d^-} k \right\} \quad (20)$$

and

$$(\hat{b}, \hat{d}) = \underset{1 \leq b \leq C_+, 1 \leq d \leq C_-}{\text{arg max}} \left\{ \sum_{k \in \mathcal{S}_b^+} k^2 + \sum_{k \in \mathcal{S}_d^-} k^2 \right\} \quad (21)$$

where $\text{arg zero}\{\cdot\}$ returns the argument which makes the enclosed objective function zero, $\mathcal{S}_b^+ \subset \mathcal{S}^+$ and $\mathcal{S}_d^- \subset \mathcal{S}^-$ stand for the possible combinatorial subset whose elements are N_b^+ and N_d^- , respectively, and C_+ and C_- are the sum of the number of combinations choosing g subcarriers from C_+ and C_- subcarriers respectively given by

$$C_+ = \sum_{g=1}^{N^+} \binom{N^+}{g} \quad \text{and} \quad C_- = \sum_{g=1}^{N^-} \binom{N^-}{g}. \quad (22)$$

With the use of the searched subsets from Equations (20) and (22), the proposed LSE of CFO and SFO can be shown to be of the following forms:

$$\hat{\varepsilon} = \frac{1}{2\pi\rho N_p} \left(\sum_{k \in \mathcal{S}_b^+} \angle \tilde{Y}_l(k) + \sum_{k \in \mathcal{S}_d^-} \angle \tilde{Y}_l(k) \right) \quad (23)$$

and

$$\hat{\zeta} = \frac{1}{2\pi\rho M_p} \left(\sum_{k \in \mathcal{S}_b^+} k \angle \tilde{Y}_l(k) + \sum_{k \in \mathcal{S}_d^-} k \angle \tilde{Y}_l(k) \right), \quad (24)$$

which indicates that the MSE performance of the CFO estimation method is primarily enhanced in proportion to N_p , whereas both the number and locations of CPs determine the performance of the SFO estimation method.

4.2. MSE Analysis

Next, the analytical expression for MSE of Equations (23) and (24) is obtained in the multipath fading channel. For notational convenience, we may rewrite Equation (10) as

$$\tilde{Y}_l(k) = |H_l(k)|^2 E_X^2 e^{j2\pi\varphi(k)\rho} \left[1 + \frac{\{\tilde{C}_l(k) + \tilde{Z}_l(k)\} e^{-j2\pi\varphi(k)\rho}}{|H_l(k)|^2 E_X^2} \right] \quad (25)$$

where $|H_l(k)|^2 = \sum_{r=1}^{N_R} |H_l^r(k)|^2$, $\tilde{C}_l(k) = \sum_{r=1}^{N_R} \tilde{C}_l^r(k)$, and $\tilde{Z}_l(k) = \sum_{r=1}^{N_R} \tilde{Z}_l^r(k)$. Since CPs are transmitted at a boosted power level of 8.52 dB, under high SNR condition, one safely assumes that

$$\angle \tilde{Y}_l(k) \approx 2\pi\varphi(k)\rho + \frac{\hat{C}_l^Q(k) + \hat{Z}_l^Q(k)}{|H_l(k)|^2 E_X^2} \quad (26)$$

where $\hat{C}_l(k) = \tilde{C}_l(k)e^{-j2\pi\varphi(k)\rho}$ and $\hat{Z}_l(k) = \tilde{Z}_l(k)e^{-j2\pi\varphi(k)\rho}$. Notice that $\hat{C}_l(k)$ and $\hat{Z}_l(k)$ are statistically identical to $\tilde{C}_l(k)$ and $\tilde{Z}_l(k)$, respectively.

With the use of optimal subsets \mathcal{S}_b^+ and \mathcal{S}_d^- , the estimation error for ε and ξ is computed by

$$\hat{\varepsilon} - \varepsilon = \frac{1}{2\pi\rho N_p E_X^2} \sum_{k \in \mathcal{S}_b^+ \cup \mathcal{S}_d^-} \frac{\hat{C}_l^Q(k) + \hat{Z}_l^Q(k)}{|H_l(k)|^2} \quad (27)$$

and

$$\hat{\xi} - \xi = \frac{1}{2\pi\rho M_p E_X^2} \sum_{k \in \mathcal{S}_b^+ \cup \mathcal{S}_d^-} \frac{k\hat{C}_l^Q(k) + k\hat{Z}_l^Q(k)}{|H_l(k)|^2}. \quad (28)$$

Recognizing that $E\{\hat{C}_l^Q(k)\} = E\{\hat{Z}_l^Q(k)\} = 0$, we obtain the following expressions:

$$\begin{aligned} E\{|\hat{\varepsilon} - \varepsilon|^2\} &= \left(\frac{1}{2\pi\rho N_p E_X^2}\right)^2 \sum_{k \in \mathcal{S}_b^+ \cup \mathcal{S}_d^-} E\left\{\frac{|\hat{C}_l^Q(k)|^2}{|H_l(k)|^4}\right\} \\ &\quad + \left(\frac{1}{2\pi\rho N_p E_X^2}\right)^2 \sum_{k \in \mathcal{S}_b^+ \cup \mathcal{S}_d^-} E\left\{\frac{|\hat{Z}_l^Q(k)|^2}{|H_l(k)|^4}\right\} \end{aligned} \quad (29)$$

and

$$\begin{aligned} E\{|\hat{\xi} - \xi|^2\} &= \left(\frac{1}{2\pi\rho M_p E_X^2}\right)^2 \sum_{k \in \mathcal{S}_b^+ \cup \mathcal{S}_d^-} k^2 E\left\{\frac{|\hat{C}_l^Q(k)|^2}{|H_l(k)|^4}\right\} \\ &\quad + \left(\frac{1}{2\pi\rho M_p E_X^2}\right)^2 \sum_{k \in \mathcal{S}_b^+ \cup \mathcal{S}_d^-} k^2 E\left\{\frac{|\hat{Z}_l^Q(k)|^2}{|H_l(k)|^4}\right\}. \end{aligned} \quad (30)$$

By placing the antennas sufficiently apart, the channel between all transmit–receive antenna couples is considered to be statistically independent. Referring from Equation (11), the variance of $\hat{C}_l^Q(k)$ in Equation (29) can be readily shown to be

$$E\left\{\frac{|\hat{C}_l^Q(k)|^2}{|H_l(k)|^4}\right\} = E_X^3 \sigma_C^2 \sum_{r=1}^{N_R} E\left\{\frac{|H_l^r(k)|^2}{\left(\sum_{r=1}^{N_R} |H_l^r(k)|^2\right)^2}\right\} + N_R E_X^2 \sigma_C^2 E\left\{\frac{1}{|H_l(k)|^4}\right\} \left(\sigma_Z^2 + \frac{\sigma_C^2}{2}\right) \quad (31)$$

where the first expectation of the RHS is further derived into

$$\begin{aligned} \sum_{r=1}^{N_R} E\left\{\frac{|H_l^r(k)|^2}{\left(\sum_{r=1}^{N_R} |H_l^r(k)|^2\right)^2}\right\} &= E\left\{\sum_{r=1}^{N_R} \frac{|H_l^r(k)|^2}{\left(\sum_{r=1}^{N_R} |H_l^r(k)|^2\right)^2}\right\} \\ &= E\left\{\frac{\sum_{r=1}^{N_R} |H_l^r(k)|^2}{\left(\sum_{r=1}^{N_R} |H_l^r(k)|^2\right)^2}\right\} \\ &= E\left\{\frac{1}{\sum_{r=1}^{N_R} |H_l^r(k)|^2}\right\}. \end{aligned} \quad (32)$$

Putting Equation (32) into Equation (31) leads to

$$E \left\{ \frac{|\hat{C}_l^Q(k)|^2}{|H_l(k)|^4} \right\} = E_X^3 \sigma_C^2 E \left\{ \frac{1}{|H_l(k)|^2} \right\} + N_R E_X^2 \sigma_C^2 E \left\{ \frac{1}{|H_l(k)|^4} \right\} \left(\sigma_Z^2 + \frac{\sigma_C^2}{2} \right). \quad (33)$$

Using Equation (32), the variance of $\hat{Z}_l^Q(k)$ in Equation (29) can be similarly calculated by

$$E \left\{ \frac{|\hat{Z}_l^Q(k)|^2}{|H_l(k)|^4} \right\} = E_X^3 \sigma_Z^2 E \left\{ \frac{1}{|H_l(k)|^2} \right\} + N_R E_X^2 \frac{\sigma_Z^4}{2} E \left\{ \frac{1}{|H_l(k)|^4} \right\}. \quad (34)$$

Since $|H_l(k)|^2$ in Equation (25) is non-centrally chi-square distributed having $2N_R$ degrees of freedom, one obtains that $E\{1/|H_l(k)|^2\} = 1/(N_R - 1)/\sigma_H^2$ for $N_T > 1$ and

$$E \left\{ \frac{1}{|H_l(k)|^4} \right\} = \begin{cases} \frac{E_1(p_{min}/\sigma_H^2)}{\sigma_H^4}, & N_R = 2 \\ \frac{1}{(N_R - 1)(N_R - 2)\sigma_H^4}, & N_R > 2 \end{cases} \quad (35)$$

where $E_1(x) = \int_x^\infty e^{-t}/t dt$ is the exponential integral.

Combining Equations (33) and (34) with Equation (35), the MSE expression of the joint frequency-offset estimator can be respectively obtained by

$$E \left\{ |\hat{\varepsilon} - \varepsilon|^2 \right\} = \frac{1}{4\pi^2 \rho^2 N_p} \left(\frac{G_1}{\gamma_z} + \frac{G_2}{2\gamma_z^2} \right) + \frac{1}{4\pi^2 \rho^2 N_p} \left(\frac{G_1}{\gamma_c} + \frac{G_2}{\gamma_z \gamma_c} + \frac{G_2}{2\gamma_c^2} \right) \quad (36)$$

and

$$E \left\{ |\hat{\xi} - \xi|^2 \right\} = \frac{1}{4\pi^2 \rho^2 M_p} \left(\frac{G_1}{\gamma_z} + \frac{G_2}{2\gamma_z^2} \right) + \frac{1}{4\pi^2 \rho^2 M_p} \left(\frac{G_1}{\gamma_c} + \frac{G_2}{\gamma_z \gamma_c} + \frac{G_2}{2\gamma_c^2} \right) \quad (37)$$

where $\gamma_z = \sigma_H^2 E_X / \sigma_Z^2$ is the average SNR, $\gamma_c = \sigma_H^2 E_X / \sigma_C^2$ is the average signal-to-ICI ratio, $G_1 = 1/(N_R - 1)$ for $N_T > 1$, and G_2 is defined as

$$G_2 = \begin{cases} E_1(p_{min}/\sigma_H^2) N_R, & N_T = 2 \\ \frac{N_R}{(N_R - 1)(N_R - 2)}, & N_T > 2 \end{cases}. \quad (38)$$

As a benchmark to the proposed scheme, similarly, the MSE of Equations (14) and (15) can be calculated by

$$E \left\{ |\hat{\varepsilon} - \varepsilon|^2 \right\} = \frac{1}{4\pi^2 \rho^2 N_f} \left(\frac{G_1}{\gamma_z} + \frac{G_2}{2\gamma_z^2} \right) + \frac{1}{4\pi^2 \rho^2 N_f} \left(\frac{G_1}{\gamma_c} + \frac{G_2}{\gamma_z \gamma_c} + \frac{G_2}{2\gamma_c^2} \right) + \left(\frac{\xi A_f}{N_f} \right)^2 \quad (39)$$

and

$$E \left\{ |\hat{\xi} - \xi|^2 \right\} = \frac{1}{4\pi^2 \rho^2 M_f} \left(\frac{G_1}{\gamma_z} + \frac{G_2}{2\gamma_z^2} \right) + \frac{1}{4\pi^2 \rho^2 M_f} \left(\frac{G_1}{\gamma_c} + \frac{G_2}{\gamma_z \gamma_c} + \frac{G_2}{2\gamma_c^2} \right) + \left(\frac{\varepsilon A_f}{M_f} \right)^2. \quad (40)$$

4.3. Computational Complexity

In this section, the complexity of the frequency-offset estimation schemes is discussed in terms of the number of arithmetic operations. The conventional scheme requires $3N_R N_f$ complex multiplications and $(N_R - 1)N_f$ complex additions to compute Equation (10). In Equations (14) and (15), $N_f + 1$ real multiplications and $2N_f - 2$ real additions are needed for each couple $(\hat{\varepsilon}, \hat{\xi})$. Since the proposed scheme uses only N_p pilot symbols selected from N_f full pilot symbols, the computational processing required in the proposed method can be identical to that used in the existing method, replacing N_f with N_p . Table 1 compares the computational complexity between the existing and proposed methods. One readily find that the computational burden of the proposed method is lower than that of the conventional method because $N_p \leq N_f$.

Table 1. Arithmetic operations of the frequency-offset estimation schemes.

Algorithm	Complex Multiplication	Complex Addition	Real Multiplication	Real Addition
Conventional	$3N_R N_f$	$(N_R - 1)N_f$	$N_f + 1$	$2N_f - 2$
Proposed	$3N_R N_p$	$(N_R - 1)N_p$	$N_p + 1$	$2N_p - 2$

5. Simulation Results and Discussions

The performance of the joint LSE schemes is assessed in the MIMO-OFDM ATSC system. The main system parameters of the ATSC 3.0 are summarized in Table 2. In this work, we have considered 8 k and 16 k modes. The signal bandwidth of 6 MHz and the sampling interval of $T = 0.14468 \mu\text{s}$ are considered [10]. In the simulations, 6-path Hilly Terrain channel model whose maximum delay is $17.2 \mu\text{s}$ is adopted [40], and the multipath channel is implemented according to Equation (5). In this channel model, the multipath intensity profile of the channel is characterized by two clusters, where each cluster is exponentially decreasing in delay. Table 3 summarizes the channel profile of 6-path Hilly Terrain channel model. To demonstrate the exactness of the MSE analysis, Doppler effects due to mobility are excluded in the adopted channel model. To find the optimal subset simultaneously meeting the constraint of Equations (20) and (22), we perform an exhaustive search over all combinations of possible subsets, and it is thereby obtained that $N_p = 45$ for 8 k mode and $N_p = 92$ for 16 k mode. In the sequel, the selected mode-specific values of N_p are used for the proposed estimation scheme.

Table 2. System parameters.

Parameters	8 k Mode	16 k Mode	32 k Mode
FFT size N	8192	16,384	32,768
sampling time T (μs)	0.14468	0.14468	0.14468
Subcarrier spacing $1/NT$ (Hz)	843.75	421.875	210.9375
Number of used subcarriers N_u	6913	13,825	27,649
Number of GI samples N_g	512	1024	2048
Number of CPs N_f	48	96	192

Table 3. Channel profiles.

Path No.	Propagation Delay	Path Power (dB)	Doppler PSD
0	0.0 μs	0	Jakes
1	0.1 μs	−1.5	Jakes
2	0.3 μs	−4.5	Jakes
3	0.5 μs	−7.5	Jakes
4	15.0 μs	−8.0	Gaus II
5	17.2 μs	−17.7	Gaus II

Figure 2 depicts a comparison between the numerical and simulated results of the frequency-offset estimation schemes when $\varepsilon = 0.05$, $\zeta = 50$ ppm, and 8 k mode is used. The probability of Rayleigh distributed random variable $|H_l^{m,r}(k)|$ larger than a minimum level p_{min} is e^{-p_{min}/σ_H^2} so that 99.9% level of Rayleigh fading is realized in the case of $p_{min}/\sigma_H^2 = -30$ dB, which is used to obtain the MSE in the case of $N_R = 2$. One can find that there is an excellent match between the numerical results and those given by the simulation in the multipath fading channel except at low SNR values. It is evident that the use of optimal subsets makes the proposed LSE achieve a better performance over the conventional LSE. In the case of SFO, it is observed that the ICI becomes a dominant term in comparison with that of an unwanted bias from the use of CPs. Especially, the performance of the proposed scheme becomes slightly degraded due to the reduced number of pilot symbol when SNR < 15 dB, whereas its performance is improved thanks to the optimal subset selection at 15 dB or higher, compared to that of the conventional scheme.

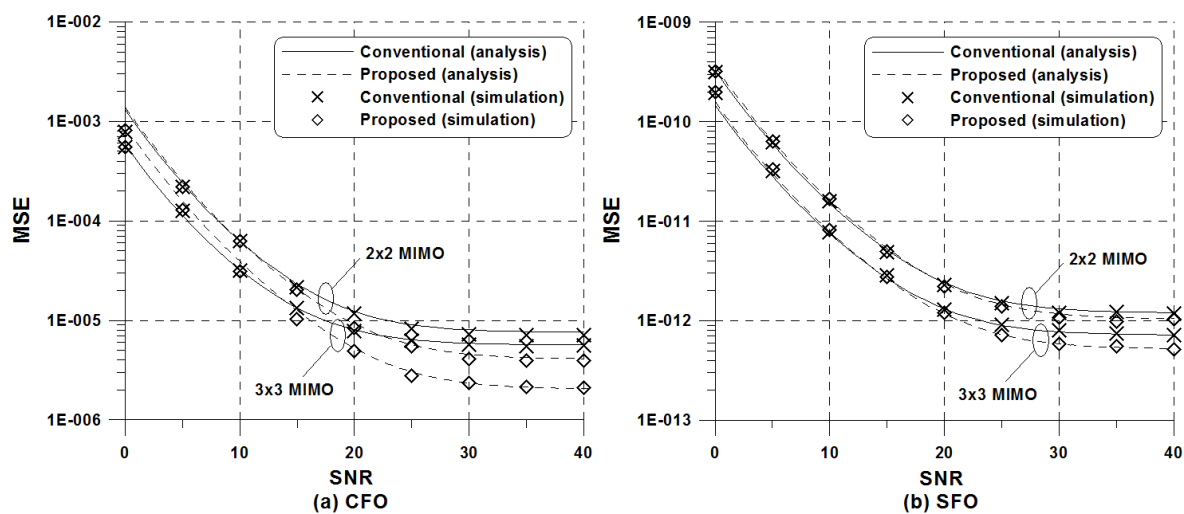


Figure 2. MSE of the frequency-offset estimators in the ATSC 8 k mode when $\varepsilon = 0.05$ and $\zeta = 50$ ppm: (a) CFO estimation; (b) SFO estimation.

Figure 3 shows the MSE of the frequency-offset estimation schemes using 16k mode. At a high SNR regime, an irreducible MSE floor introduced by frequency-offset induced ICI is observed in the frequency estimation schemes. Because of the non-symmetrical distribution of CPs, the MSE performance of the conventional scheme using full CPs exhibits a severe error floor, which decreases with increasing N_R , compared to that of the proposed scheme. Therefore, the pilot subset selection serves to remove a bias resulting from the use of randomly distributed CPs, and the MSE can be minimized by the proper selection of pilot subset. As expected in Equations (36) and (37), the detection ability can be enhanced with N_R . Such physical behaviors is attributed to the fact that the use of multiple receive antennas increases the number of statistically independent observation samples used for frequency-offset estimation. More importantly, the performance gap between the conventional and proposed scheme becomes remarkable as N_R increases.

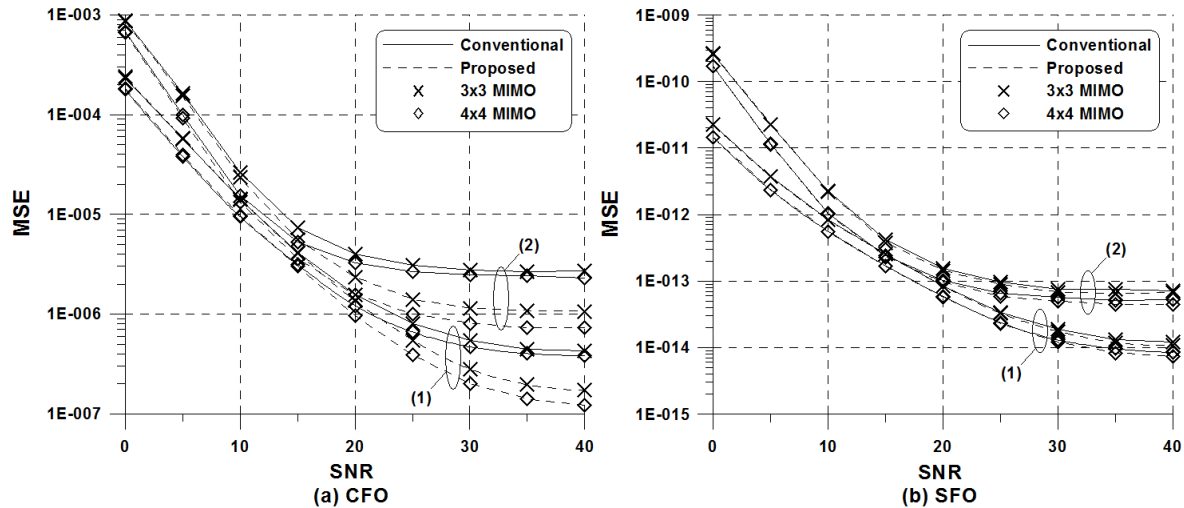


Figure 3. MSE of the frequency-offset estimation schemes in the ATSC 16 k mode: (1) $\varepsilon = 0.02$ and $\zeta = 20$ ppm; (2) $\varepsilon = 0.05$ and $\zeta = 50$ ppm; (a) CFO estimation; (b) SFO estimation.

Figures 4 and 5 present the MSE of the CFO detection methods for different values of frequency offsets when 8k and 16k modes are used, respectively. Here, the SNR was fixed at 30 dB. It is obvious from the figure that the increase in frequency offset induces a significant ICI as well as an additional bias in the case of the conventional scheme. More specifically, the increase in SFO heavily affects the MSE of the conventional scheme, whereas the proposed scheme turns out to be insensitive to the amount of SFO. For a wider fractional CFO range, it is also observed that theoretical analysis is in perfect agreement with simulated results. As predicted, the presence of multiple receive antennas enhances frequency-estimation performance due to inherent spatial diversity. In the case of the conventional scheme, the effect of receive diversity becomes outstanding for large values of CFO, whereas the same diversity effect of the proposed method is achieved regardless of the value of CFO in the case of the proposed scheme. Since CFO is very small during the tracking phase, the proposed estimation method is effective for MIMO-OFDM system and copes better with intrinsic ICI than the conventional method using full CPs.

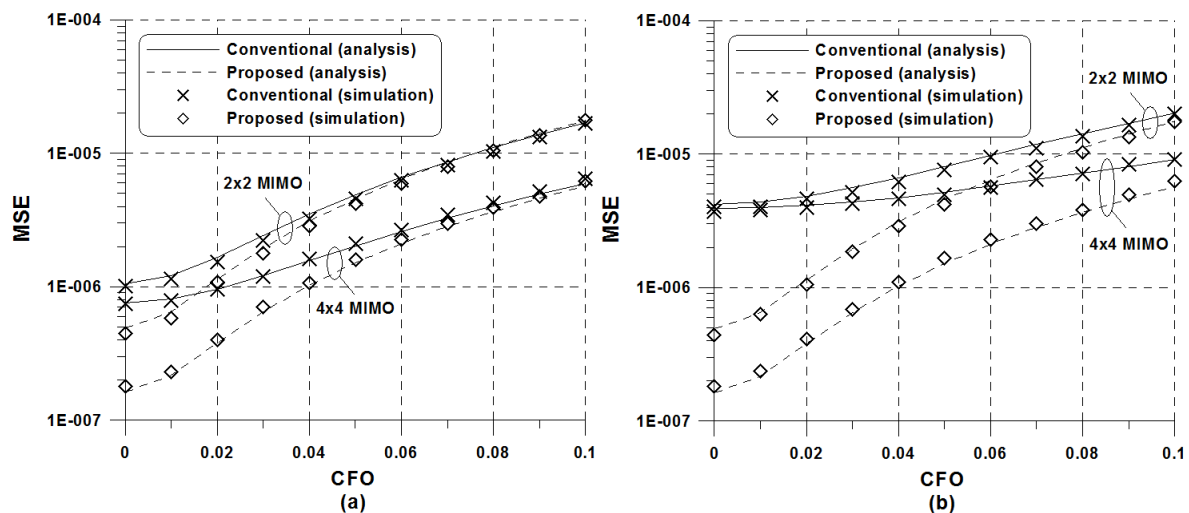


Figure 4. MSE of the CFO estimators versus offsets in the ATSC 8 k mode when SNR = 30 dB: (a) $\zeta = 20$ ppm; (b) $\zeta = 50$ ppm.

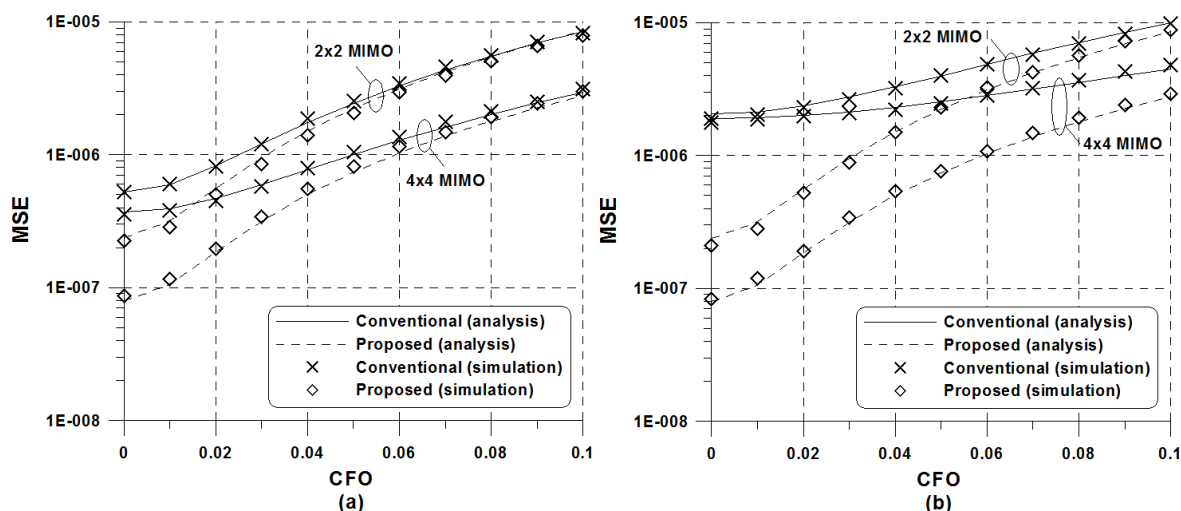


Figure 5. MSE of the CFO estimators versus offsets in the ATSC 16 k mode when SNR = 30 dB: (a) $\xi = 20$ ppm; (b) $\xi = 50$ ppm.

6. Conclusions

For reliable operation of OFDM systems, it is important to perform frequency-offset estimation robustly. Addressing this issue, this paper proposed an effective joint CFO and SFO estimation method in the ATSC system using MIMO-OFDM. For this purpose, a pilot subset selection was deployed on a per-subcarrier basis so that the proposed joint LSE was implemented in a decoupled way. To demonstrate the usefulness of the joint LSE approach, the MSE performance was numerically derived in a multipath fading channel considering the MIMO-OFDM context. By deriving a closed-form expression for the MSE of the frequency-offset estimate, it was shown the MIMO-OFDM ATSC system has a rich structural information to synchronize a system. The proposed joint estimation scheme that benefits from the optimal pilot subset was proven to be less affected by the amount of frequency offsets and to be computationally inexpensive, as compared to the conventional estimation scheme. Therefore, the proposed frequency-offset estimation scheme can be used to maximize the benefits of MIMO-OFDM in digital multimedia terrestrial broadcast systems. In future works, the presented theoretical analysis could be straightforwardly applied to other multimedia terrestrial broadcast systems. In addition, the performance of the MIMO-OFDM ATSC system under realistic channel conditions would reinforce the numerical analysis, particularly taking into account scenarios where the channels between transmit–receive antenna couples are correlated.

Author Contributions: Y.-A.J. developed the estimation method and conducted computer simulations. Y.-H.Y. analyzed the performance of the presented detection method and verified numerical results.

Funding: This research was supported by the Basic Science Research Program through the National Research Foundation of Korea (NRF) funded by the Ministry of Education (NRF-2018R1D1A1B07048819).

Conflicts of Interest: The authors declare no conflict of interest.

References

1. Cvijetic, N. OFDM for next-generation optical access networks. *J. Lightw. Technol.* **2012**, *30*, 384–398. [\[CrossRef\]](#)
2. Shimizu, S.; Cincotti, G.; Wada, N. Demonstration and performance investigation of all-optical OFDM systems based on arrayed waveguide gratings. *Opt. Express* **2012**, *20*, 525–534. [\[CrossRef\]](#) [\[PubMed\]](#)
3. Arik, S.O.; Kahn, J.M.; Ho, K. MIMO signal processing for mode-division multiplexing: An overview of channel models and signal processing architectures. *IEEE Signal Process. Mag.* **2014**, *31*, 25–34. [\[CrossRef\]](#)
4. Elbaz, D.; Malka, D.; Zalevsky, Z. Photonic crystal fiber based 1xN intensity and wavelength splitters/couplers. *Electromagnetics* **2012**, *32*, 209–220. [\[CrossRef\]](#)
5. Vappangi, S.; Mani Vakamulla, V. Synchronization in visible light communication for smart cities. *IEEE Sens. J.* **2018**, *18*, 1877–1886. [\[CrossRef\]](#)

6. ETSI ES 201 980 V4.1.1. Digital radio mondiale (DRM); System Specification; European Broadcasting Union, 2014. Available online: <http://www.dvb.org/> (accessed on 20 August 2018).
7. ETSI EN 302 755 V1.4.1. Digital video broadcasting (DVB); Frame Structure Channel Coding and Modulation for a Second Generation Digital Terrestrial Television Broadcasting System (DVB-T2); European Broadcasting Union, 2015. Available online: <http://www.dvb.org/> (accessed on 20 August 2018).
8. DVB Document A160. Digital Video Broadcasting, Next Generation Broadcasting System to Handheld, Physical Layer Specification (DVB-NGH); European Broadcasting Union, 2012. Available online: <http://www.dvb.org/> (accessed on 20 August 2018).
9. ITU-R. WP 11A/59. Channel Coding, Frame Structure and Modulation Scheme for Terrestrial Integrated Service Digital Broadcasting (ISDB-T), 1999. Available online: <https://www.arib.or.jp/> (accessed on 20 August 2018).
10. Document A/322. ATSC Standard: Physical Layer Protocol; Advanced Television Systems Committee: Washington, DC, USA, 2017. Available online: <https://www.atsc.org/> (accessed on 20 August 2018).
11. Hossen, M.S.; Kim, S.H.; Kim, K.D. Stereoscopic video transmission over DVB-T2 system using future extension frame. *IEEE Trans. Broadcast.* **2016**, *62*, 817–825.
12. Gomez-Barquero, D.; Douillard, C.; Moss, P.; Mignone, V. DVB-NGH: The next generation of digital broadcast services to handheld devices. *IEEE Trans. Broadcast.* **2014**, *60*, 246–257. [[CrossRef](#)]
13. Gomez-Barquero, D.; Vargas, D.; Fuentes, M.; Klenner, P.; Moon, S.; Choi, J.; Schneider, D.; Murayama, K. MIMO for ATSC 3.0. *IEEE Trans. Broadcast.* **2016**, *62*, 298–305. [[CrossRef](#)]
14. Saito, S.; Shitomi, T.; Asakura, S.; Satou, A.; Okano, M.; Murayama, K.; Tsuchida, K. 8K terrestrial transmission field tests using dual-polarized MIMO and higher-order modulation OFDM. *IEEE Trans. Broadcast.* **2016**, *62*, 306–315. [[CrossRef](#)]
15. Shitomi, T.; Garro, E.; Murayama, K.; Gomez-Barquero, D. MIMO scattered pilot performance and optimization for ATSC 3.0. *IEEE Trans. Broadcast.* **2018**, *64*, 188–200. [[CrossRef](#)]
16. Vargas, D.; Kim, Y.; Bajcsy, J.; Gomez-Barquero, D.; Cardona, N. A MIMO-channel-precoding scheme for next generation terrestrial broadcast TV systems. *IEEE Trans. Broadcast.* **2015**, *61*, 445–456. [[CrossRef](#)]
17. Speth, M.; Fechtel, S.A.; Fock, G.; Meyr, H. Optimum receiver design for wireless broad-band systems using OFDM-Part I. *IEEE Trans. Commun.* **1999**, *47*, 1668–1677. [[CrossRef](#)]
18. Rotoloni, M.; Tomasin, S.; Vangelista, L. Maximum likelihood estimation of time and carrier frequency offset for DVB-T2. *IEEE Trans. Broadcast.* **2012**, *58*, 77–86. [[CrossRef](#)]
19. Zhang, J.; Tian, L.; Wang, Y.; Liu, M. Selection transmitting/maximum ratio combining for timing synchronization of MIMO-OFDM systems. *IEEE Trans. Broadcast.* **2014**, *60*, 626–636. [[CrossRef](#)]
20. Surantha, N.; Nagao, Y.; Kurosaki, M.; Ochi, H. Sampling frequency offset estimation for digital terrestrial television broadcasting system. *IEICE Commun. Express* **2013**, *2*, 224–230. [[CrossRef](#)]
21. Fay, L.; Michael, L.; Gomez-Barquero, D.; Ammar, N.; Caldwell, M. An overview of the ATSC 3.0 physical layer specification. *IEEE Trans. Broadcast.* **2016**, *62*, 159–171. [[CrossRef](#)]
22. Oberli, C. ML-based tracking algorithms for MIMO-OFDM. *IEEE Trans. Wirel. Commun.* **2007**, *6*, 2630–2639. [[CrossRef](#)]
23. Jose, R.; Hari, K.V.S. Maximum likelihood algorithms for joint estimation of synchronisation impairments and channel in multiple input multiple output orthogonal frequency division multiplexing system. *IET Commun.* **2013**, *7*, 1567–1579. [[CrossRef](#)]
24. Yuan, J.; Torlak, M. Joint CFO and SFO estimator for OFDM receiver using common reference frequency. *IEEE Trans. Broadcast.* **2016**, *62*, 141–149. [[CrossRef](#)]
25. Kim, Y.H.; Lee, J.H. Joint maximum likelihood estimation of carrier and sampling frequency offsets for OFDM systems. *IEEE Trans. Broadcast.* **2013**, *57*, 277–283.
26. Speth, M.; Fechtel, S.A.; Fock, G.; Meyr, H. Optimum receiver design for OFDM-based broadband transmission-Part II: a case study. *IEEE Trans. Commun.* **2001**, *49*, 571–578. [[CrossRef](#)]
27. Shi, K.; Serpedin, E.; Ciblat, P. Decision-directed fine synchronization in OFDM systems. *IEEE Trans. Commun.* **2005**, *53*, 408–412. [[CrossRef](#)]
28. Liu, S.; Chong, J.A. Study of joint tracking algorithms of carrier frequency offset and sampling clock offset for OFDM-based WLANs. In Proceedings of the International Conference on Communications, Circuits and Systems and West Sino Expositions, Chengdu, China, 29 June–1 July 2002.

29. Tsai, P.Y.; Kang, H.Y.; Chiueh, T.D. Joint weighted least-squares estimation of carrier-frequency offset and timing offset for OFDM systems over multipath fading channels. *IEEE Trans. Veh. Technol.* **2005**, *54*, 211–223. [[CrossRef](#)]
30. Chiang, P.H.; Lin, D.B.; Li, H.J.; Stuber, G. L. Joint estimation of carrier-frequency and sampling-frequency offsets for SC-FDE systems on multipath fading channels. *IEEE Trans. Commun.* **2008**, *56*, 1231–1235. [[CrossRef](#)]
31. Lin, Y.T.; Chen, S.G. A blind fine synchronization scheme for SC-FDE systems. *IEEE Trans. Commun.* **2014**, *62*, 293–301. [[CrossRef](#)]
32. Nguyen-Le, H.; Le-Ngoc, T.; Ko, C.C. Joint channel estimation and synchronization for MIMO-OFDM in the presence of carrier and sampling frequency offsets. *IEEE Trans. Veh. Technol.* **2009**, *58*, 3075–3081. [[CrossRef](#)]
33. Morelli, M.; Moretti, M. Fine carrier and sampling frequency synchronization in OFDM systems. *IEEE Trans. Wireless Commun.* **2010**, *9*, 1514–1524. [[CrossRef](#)]
34. Murin, Y.; Dabora, R. Low complexity estimation of carrier and sampling frequency offsets in burst-mode OFDM systems. *Wireless Commun. Mob. Comput.* **2016**, *16*, 1018–1034. [[CrossRef](#)]
35. Jose, R.; Ambat, S.K.; Hari, K.V.S. Low complexity joint estimation of synchronization impairments in sparse channel for MIMO-OFDM system. *Int. J. Electron. Commun.* **2014**, *68*, 151–157. [[CrossRef](#)]
36. Salari, S.; Heydarzadeh, M. Joint maximum-likelihood estimation of frequency offset and channel coefficients in multiple-input multiple-output orthogonal frequency-division multiplexing systems with timing ambiguity. *IET Commun.* **2011**, *5*, 1964–1970. [[CrossRef](#)]
37. Yao, Y.; Giannakis, G.B. Blind carrier frequency offset estimation in SISO, MIMO, and multiuser OFDM systems. *IEEE Trans. Commun.* **2005**, *53*, 173–183. [[CrossRef](#)]
38. Lin, T.T.; Hwang, F.H. On the CFO/Channel estimation technique for MIMO-OFDM systems without using a prior knowledge of channel length. *EURASIP J. Wirel. Commun. Netw.* **2015**, *79*, 1–13. [[CrossRef](#)]
39. Salvo Rossi, P.; Romano, G.; Ciuonzo, D.; Palmieri, F. Gain design and power allocation for overloaded MIMO-OFDM systems with channel state information and iterative multiuser detection. In Proceedings of the 2011 International Symposium on Wireless Communication Systems, Aachen, Germany, 6–9 November 2011; pp. 769–773.
40. Failli, M. *COST 207: Digital Land Mobile Radio Communications*; European Commission: Luxembourg, 1989.



© 2018 by the authors. Licensee MDPI, Basel, Switzerland. This article is an open access article distributed under the terms and conditions of the Creative Commons Attribution (CC BY) license (<http://creativecommons.org/licenses/by/4.0/>).